

Allylic H-Abstraction Mechanism: The Potential Energy Surface of the Reaction of Propene with OH Radical

Milan Szori,[†] Christa Fittschen,[‡] Imre G. Csizmadia,^{†,§} and Bela Viskolcz^{*,†}

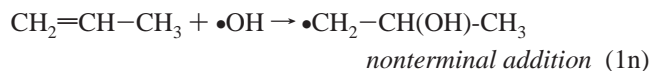
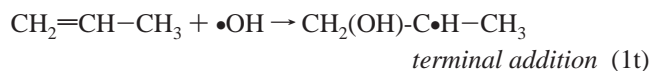
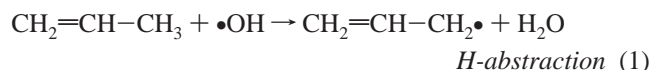
Department of Chemistry and Chemical Informatics, Faculty of Education,
University of Szeged, Szeged, Boldogasszony sgt. 6, Hungary 6725, PhysicoChimie des
Processus de Combustion et de l'Atmosphère - UMR 8522, Centre d'Etudes et de
Recherches Lasers et Applications Université de Lille 1, F-59655 Villeneuve d'Ascq,
Cedex, France, and Department of Chemistry, University of Toronto,
Toronto, Ontario, Canada M5S 3H6

Received April 13, 2006

Abstract: The allylic H-atom abstraction reaction plays a more dominant role, especially at lower temperature, than addition reactions in the case of the $\text{CH}_2=\text{CH}-\text{CH}_3 + \bullet\text{OH}$ system. Different computational methods including ab initio as well as density functional methods have been used to examine allylic H-abstraction. Both the energetically less favorable direct H-abstraction and the more favorable indirect H-abstractions have been investigated. Using first principles computations, for the indirect abstraction, a stable π - or reactantlike as well as a late productlike complex were found on the potential energy surface. Based on higher level single point calculations (QCISD(T)/6-311+G(3df,2p)), a new activation enthalpy value, $\Delta^\ddagger H^\circ = 0.3 \pm 2$ kJ/mol, is suggested for the title reaction. The computed reaction enthalpy $\Delta_r H^\circ = -124.7 \pm 2$ kJ/mol is in good agreement with the experimental value. The stability of the initial π -complex was found to be $\Delta H^\circ_{\pi\text{-complex}} = -7.1$ kJ/mol. The product complex between the transition state and the product was found with the stability of -127.2 kJ/mol.

1. Introduction

Many radical-molecule reactions exhibit negative activation energies, such as the addition of OH radical¹ or Cl atom to olefins.² The situation becomes more complicated in the case of substituted olefins, like propene. H-atom abstraction (1) may play an important role in the overall kinetics besides reaction channels of the terminal (1t) and nonterminal (1n) additions, both of which lead to the formation of hydroxy-alkyl radicals:³



Despite what is mentioned above, the dominance of quasi barrierless additional channels was reported in several cases.⁴ However, H-abstraction reactions are critical in complex reaction systems such as the combustion of hydrocarbon fuels,⁵ atmospheric chemistry,⁶ and autoignition⁷ as well as various processes of biological systems.⁸ During the past few decades, OH radical reactions involving different organic compounds were of special interest in gas-phase kinetic studies.^{9–11} The most recent experimental study focused upon reactions used in the detection of OH radical decay at low temperatures by laser induced fluorescence (LIF) spectroscopy.¹² The branching ratios of elementary steps in most

* Corresponding author e-mail: viskolcz@jgytf.u-szeged.hu.

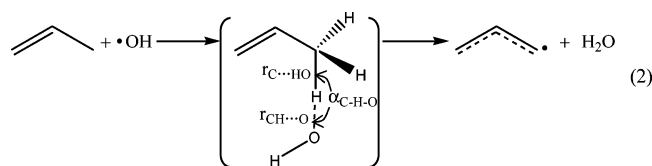
[†] University of Szeged.

[‡] Centre d'Etudes et de Recherches Lasers et Applications Université de Lille 1.

[§] University of Toronto.

cases were not distinguishable by a direct technique where only one species is detected. If a chemical system is small enough, then ab initio calculations may be utilized to produce an accurate reactive potential energy surface (PES),¹³ thus permitting current chemical reaction rate theories to be tested. Besides extensive experimental studies,^{14,15} a number of theoretical calculations were carried out on the elementary steps involving the reaction for the OH radical with different unsaturated hydrocarbons.¹⁶ The reaction of the simplest system ($\text{H}_2\text{C}=\text{CH}_2 + \text{OH}$) has been studied extensively.^{17–19} However, propene is the next step toward the understanding of OH reaction with the unsaturated hydrocarbon homologue, and only a few theoretical studies have been reported for the propene + OH system.^{20,21} Surprisingly, H-atom abstraction has not yet been studied using high level quantum chemistry calculations, and neither have theoretical comparisons with addition channels been well established.

Allylic hydrogen may be extracted via two possible H-atom abstraction channels which can play a significant role in the overall kinetics of the OH and propene system. One of them, indirect abstraction, can start from a so-called π -complex, the other is the direct H-abstraction. Higher unsaturated hydrocarbons (including higher degrees of unsaturation) react with OH radicals, via additions, as well as hydrogen atom abstractions.²² A prototype of the allylic H-abstraction is shown in eq 2:



For an indirect abstraction the central structure in square brackets in eq 2 would be a minimum energy structure labeled as a reactant (or π) complex. For a direct abstraction it would be a transition state.

Both QCISD and CCSD theoretical models yield results that have been shown to be relatively stable with regard to a modest spin contamination in the unrestricted case.²³ Radom et al. suggested that UMP2 should be used with caution, since this method is too erratic for general use for radicals.²⁴ The density functional theory (DFT), which uses gradient-corrected exchange and correlation potentials, has been shown to be an efficient and accurate tool to calculate molecular properties such as structural geometry and vibrational frequencies.^{25–28} The unrestricted DFT wave function is typically considerably less spin contaminated than the corresponding UHF wave function for a given open shell system.^{29,30} A number of DFT transition state property studies have been carried out^{31,32} and assessed by comparing the computed results with experimental and other theoretical results.

In the present paper, different computational methods were applied and analyzed for similarities and differences in their respectively computed PESs. One of the aims of this study is to test systematically the different levels of theory for their efficiency and accuracy with respect to the given system and, furthermore, to demonstrate the importance of the allylic

H-atom abstraction. One has to note that some comparisons were published previously,^{33,34} for a similar type of reaction. The experience gained will help to choose a suitable method for describing hydrogen abstraction reactions from unsaturated hydrocarbons and their derivatives such as polyunsaturated fatty acids (PUFA).

2. Computational Methods

To generate potential energy surfaces (PESs), in the vicinity of the H-abstraction transition state, relaxed scans were carried out by systematically altering two variables, namely $r_{\text{C}\cdots\text{HO}}$ (i.e. the C–H bond to be broken) and $r_{\text{CH}\cdots\text{O}}$ (i.e. the H–O bond to be formed), as shown in eq 2. Values of the $r_{\text{C}\cdots\text{HO}}$ parameter were changed between 1.1 Å and 1.3 Å, while the $r_{\text{CH}\cdots\text{O}}$ parameter was varied from 1.2 Å to 1.6 Å. The step sizes were 0.04 Å in both directions. The quadratic convergence SCF procedure³⁵ was used in each scan. The potential energy surface with all tested methods combined utilized the standard 6-31G(d) split valence basis set.³⁶

For geometry optimizations, a number of standard methods were used, namely ab initio HF,^{37–39} MP2,^{40–43} QCISD,⁴⁴ and CCSD.^{45–48} A set of density functional theory (DFT)⁴⁹ methods such as B3PW91, B1B95, B1LYP, MPW1PW91, PBE1PBE, BHandH, and BHandHLYP was also applied to characterize the transition state. Two DFT methods are presented in the present paper as two differently performing examples. These were the B3LYP^{50,51} and the BH&HLYP⁵² methods, exemplifying in geometry points of view a not very accurate and a relatively accurate DFT methods, respectively. The remaining DFT results, listed in Table S1 of the Supporting Information, show that they produce geometries scattered around the most accurate QCISD and CCSD methods (Figure 1) which also produced the best activation enthalpies for the reaction using a large basis set. The minima and saddle points of the PESs (i.e. reactants, products, complexes, and transition states) were checked by frequency analysis at each level of theory. The zero point vibrational energy (ZPVE) was scaled by standard factors.⁵³

To increase the accuracy of the computed PES, a non-iterative addition of triple excitations was taken into consideration using the QCISD(T)⁴⁴ and CCSD(T)⁴⁴ methods. The QCISD(T)-PES and the CCSD(T)-PES were mapped out by QCISD(T)/6-31G(d) and CCSD(T)/6-31G(d) single point calculations using CCSD/6-31G(d) geometries, denoted as QCISD(T)/6-31G(d)//CCSD/6-31G(d) and CCSD(T)/6-31G(d)//CCSD/6-31G(d), respectively.

Basis set effects on the electronic energy were also studied with single point calculations for the BH&HLYP method using BH&HLYP/6-31G(d) geometries and also at the QCISD(T) and CCSD(T) level of theories using CCSD/6-31G(d) and BH&HLYP geometries. Two types of split valence basis sets³⁶ were used which were also augmented with diffuse and polarization functions {6-31G(d), 6-311G-(d,p), 6-311+G(d,p), 6-311+G(3df,2p)} as well as Dunning's correlation consistent basis sets^{54–58} {cc-pVxZ, aug-cc-pVxZ (where x is D, T, and Q for cc-pVxZ and D, T for aug-cc-pVxZ)}. The effects of using these different basis sets were explored.

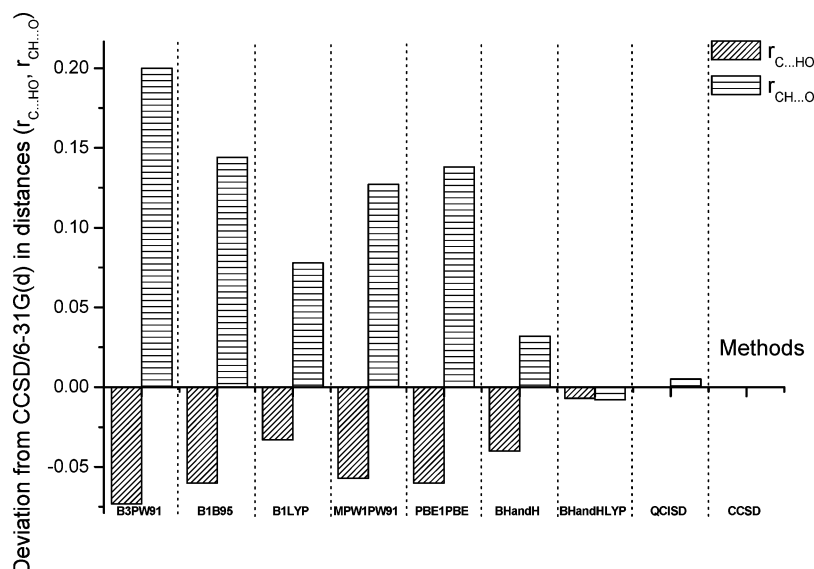


Figure 1. A comparison of different DFT methods with high level ab initio (QCISD and CCSD) calculations in terms of geometrical parameters ($r_{C...OH}$ and $r_{CH...O}$) of the H-abstraction transition state associated with the $CH_2=CHCH_3 + \bullet OH$ system.

The basis set superposition error (BSSE) is considered for the complexes by using the simple counterpoise (CP) method⁵⁹

$$\Delta E^{CP} = E^{AB} - [E^{A(AB)} + E^{B(AB)}] \quad (3)$$

where E^{AB} is the energy of the supermolecule (e.g. π -complex), $E^{A(AB)}$ is the energy of molecule A (e.g. propene) with the basis set of supermolecule AB, and $E^{B(AB)}$ is the energy of molecule B (e.g. hydroxyl radical) with the basis set of the AB supermolecule. This method was applied to the QCISD(T) and CCSD(T) single point calculations for the final analysis of the reaction profile (using "Counterpoise=2" keyword in Gaussian03).

For testing the IRCMax⁶⁰ method, calculations are carried out on the QCISD(T)/6-311+G(3df,2p)//BH&HLYP/6-31G(d) level of theory. All of the calculations were carried out using the GAUSSIAN03 program package.⁶¹

3. Scope

The allylic H-abstraction can be envisaged with the following possibilities: (i) a direct abstraction mechanism, (ii) an indirect abstraction mechanism, and (iii) a mixture of a direct and indirect abstraction mechanism.

To decide which one of the above possibilities is operative it is necessary to search for transition states. If only one TS exists, then it can be analyzed whether (i) or (ii) is the actual mechanism. If a pair of TSs are located, then (iii) is operative, and the relative barrier heights for the two TSs will predetermine which mechanism is dominantly operative as it is illustrated in Figure 2. If either (ii) or (iii) is operative, then one must search for one or two reactants or π -complexes. If only one π -complex exists, then it should be common for both the H-abstraction and the OH addition (Figure 3A). If there are two π -complexes formed, then one is for the H-abstraction and one is for the OH addition (Figure 3B): (i) one π -complex is formed which is common for both H-abstraction and OH addition (Figure 3A) and (ii) two

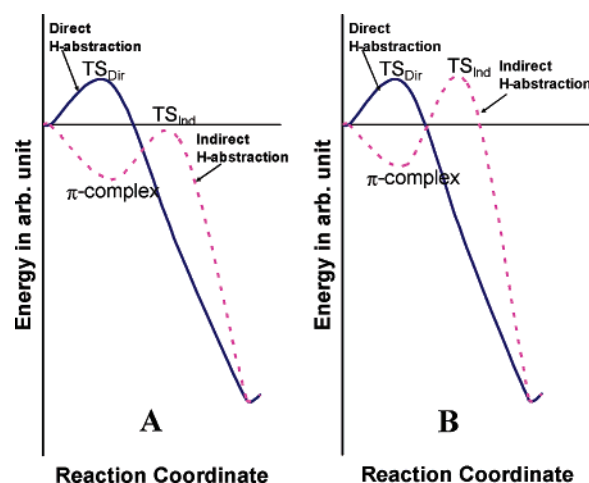


Figure 2. Two possible reaction energy profiles involving two alternative H-abstraction mechanisms showing that direct and indirect H-abstractions compete with each other. Note that TS_{Dir} is always positive, even though the barriers are usually low, while TS_{Ind} may be either positive or negative. A: indirect H-abstraction is favored because $TS_{Ind} < TS_{Dir}$ and B: direct H-abstraction is favored because $TS_{Ind} > TS_{Dir}$.

π -complexes are formed, one is for the H-abstraction and one is for the OH addition (Figure 3B).

In this paper we shall seek to answer these questions but not necessarily in the order listed above. Before all of these questions could be answered, a full exploration of the theoretical methods and basis sets applied must be carried out for the computational accuracy which will make the conclusions reliable.

4. Results and Discussion

4.1. Geometries of the Critical Points and Along the RC.

Along each path there may be several minimum energy points corresponding to either reactants, reaction intermediates, or products. This study explores the geometries of the maxima and minima along the hydrogen abstraction reaction

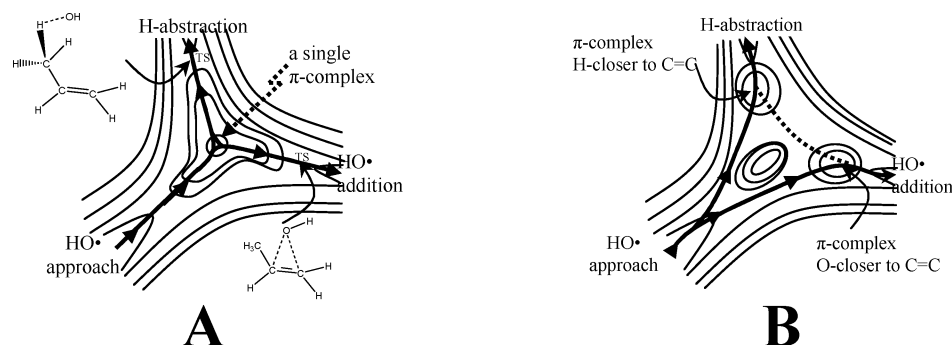
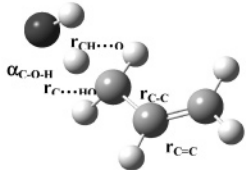


Figure 3. Model potential energy surfaces for the $\text{CH}_2=\text{CHCH}_3 + \bullet\text{OH}$ system involving addition as well as allylic H-abstraction. A: two reaction paths involving a single π -complex and B: two reaction paths involving two separate π -complexes

Table 1. Geometric Parameters of Reactants, Products, and First-Order Saddle Point (TS) Computed at the BH&HLYP/6-31G(d), QCISD/6-31G(d), and CCSD/6-31G(d) Levels of Theory and Available Experimental Results

		propene + OH				TS			allyl radical + H ₂ O			
		BH&HLYP	CCSD	QCISD	Exp.	BH&HLYP	CCSD	QCISD	BH&HLYP	CCSD	QCISD	Exp.
$r_{\text{C}=\text{C}}$	in Å	1.322	1.338	1.339	1.341 ^a	1.331	1.343	1.344	1.379	1.390	1.390	1.3869 ^c
$r_{\text{C}-\text{C}}$	in Å	1.495	1.504	1.504	1.506 ^a	1.467	1.480	1.480	1.379	1.391	1.391	1.3869 ^c
$r_{\text{C}\cdots\text{HO}}$	in Å	1.089	1.098	1.099	1.117 ^a	1.224	1.231	1.232	-	-	-	-
$\alpha_{\text{C}=\text{C}-\text{C}}$	in degree	125.1	124.7	124.7	124.3 ^a	124.5	124.1	124.1	124.8	124.4	124.4	123.96 ^c
$\alpha_{\text{C}-\text{C}-\text{H}}$	in Å	111.1	111.1	111.1	110.7 ^a	109.5	109.1	109.1	-	-	-	-
$\alpha_{\text{C}-\text{H}-\text{O}}$	in degree	-	-	-	-	173.7	171.7	171.9	-	-	-	-
$\alpha_{\text{C}=\text{C}-\text{C}-\text{H}}$	in degree	120.7	120.4	120.4	n.a.	-105.6	-104.9	-104.7	-	-	-	-
$\pi_{\text{C}(\text{C})-\text{H}-\text{O}}$	in degree	-	-	-	-	76.7	52.0	56.0	-	-	-	-
$\pi_{\text{C}-\text{H}(\text{O}-\text{H})}$	in degree	-	-	-	-	-27.9	-9.3	-12.7	-	-	-	-
$r_{\text{O}-\text{H}}$	in Å	0.969	0.984	0.984	0.971 ^b	0.966	0.981	0.981	0.957	0.970	0.970	0.9575 ^a
$\alpha_{\text{H}(\text{O}-\text{H})}$	in degree	-	-	-	-	97.9	97.2	97.1	104.6	104.0	104.0	104.51 ^a
$r_{\text{CH}\cdots\text{O}}$	in Å	-	-	-	-	1.309	1.317	1.318	0.957	0.970	0.970	0.9575 ^a

^a—cExperimental geometries from refs 62–64, respectively.

of the $\text{CH}_3\text{CH}=\text{CH}_2 + \text{OH}$ system. As pointed out in the previous section, such a path of hydrogen abstraction may be at least partially, if not completely, different from the path of the addition of the OH radical to the double bond.

4.1.1. Reactants and Products. Table 1 shows, besides the data of TS obtained initially, the calculated geometrical parameters of reactants and products at the BH&HLYP/6-31G(d), QCISD/6-31G(d), and CCSD/6-31G(d) levels of theory. Both reactants and product are in very good agreement with the available experimental data;^{62–64} the largest deviation from experimental data in the geometrical parameters of the reactants was found in the allylic C–H bond length (the bond to be broken during the reaction), but these deviations were smaller than 0.02 Å at the BH&HLYP/6-31G(d) and smaller than 0.03 Å at the CCSD/6-31G(d) level of theory. In terms of bond angle deviation, the angular deviations of the carbon chain (denoted $\alpha_{\text{C}=\text{C}-\text{C}}$) were less

than 0.8 degrees using DFT and half of that value at the CCSD level of theory. On the side of the products, the deflection between experimental and theoretical methods was about the same in the angles, and in the distance deviation it was found to be around 0.01 Å. However, it is clear that the quality of the geometry can be improved somewhat by increasing the number of basis functions, but our aim was to obtain reasonable geometries not only for this system but also for larger alkenes.

4.1.2. Potential Energy Surfaces and Location of the TS in H-Abstraction. The selected geometry parameters (namely the $r_{\text{CH}\cdots\text{O}}$, $r_{\text{C}\cdots\text{HO}}$, and $\alpha_{\text{C}-\text{H}-\text{O}}$) and enthalpies are listed and compared in Table 2 specifically for TS of the reaction 2. This demonstrates that at the HF level of theory, the TS structure is almost halfway between the reactant and product. However, high level ab initio calculations such as CCSD show that the TS became more and more reactantlike.

Table 2. Standard Reaction and Activation Enthalpies in kJ/mol and Relevant Geometrical Parameters of the Indirect H-Abstraction TS Structure for the $\text{CH}_2=\text{CHCH}_3 + \bullet\text{OH} \rightarrow \text{CH}_2=\text{CHCH}_2\bullet + \text{H}_2\text{O}$ Reaction Computed at Different Levels of Theory Using a 6-31G(d) Split Valence Basis Set

method	$\Delta_r H^\circ$	$\Delta^\ddagger H^\circ$	$r_{\text{CH}\cdots\text{O}}$ (Å)	$r_{\text{C}\cdots\text{HO}}$ (Å)	$\alpha_{\text{C-H-O}}$
B3LYP	-102.2				
HF	-70.2 ^a	88.3 ^a	1.270	1.276	176.3
MP2	-81.6 ^a	47.7 ^a	1.293	1.216	163.4
BH&HLYP	-87.9	18.8	1.309	1.224	173.7
QCISD	-89.8 ^a	30.7 ^a	1.318	1.232	171.9
CCSD	-89.2	32.0	1.317	1.231	171.6
exp.	-128.53 ^b	-3.7 ^c			

^a Values of ZPVE are scaled. Scale factors used are from ref 53.

^b The experimental reaction enthalpy is calculated from data given in refs 65–67. ^c The experimental reaction rate is published in ref 72.

Generally, the transition state structure obtained by the CCSD/6-31G(d) methods can be considered to be the most accurate geometry.

Within the coupled cluster method, the $\text{C}\cdots\text{HO}$ bond length of the TS stretched to 1.231 Å from the original 1.098 Å, amounting to an increase of 0.133 Å. However, the coupled cluster method revealed that the $\text{CH}\cdots\text{O}$ bond distance was 1.317 Å, which is about 0.347 Å away from the final H–O bond length of the product H_2O (0.970 Å). These two geometrical parameters indicate that the allylic H-atom abstraction has an early transition state. In addition, the TS corresponded to a nearly linear approach between the species, since the optimized $\alpha_{\text{C-H-O}}$ was 171.7°. The TS structures listed in Tables 1 and 2 obtained by BH&HLYP/6-31G(d) and QCISD/6-31G(d) are very similar to those found by CCSD/6-31G(d). It is important to note that this TS could not be found at the B3LYP/6-31(d) optimization level.

The differences in reaction enthalpy ($\Delta_r H^\circ$) and activation enthalpy ($\Delta^\ddagger H^\circ$) are rather large and show a marked disagreement with the experimental values as listed in Table 2. It is rather difficult to suggest that there is a convergence in energies of the different methods used up until now. All theoretical methods underestimate the reaction exothermicity by a large margin of 25–60 kJ/mol. The calculated activation enthalpy was also overestimated by about the same amount. Thus, the various methods, used so far, produced values which were too high, with respect to both in terms of thermodynamics and kinetics. To conclude, higher post-HF methods coupled with relatively small basis sets do not permit accurate calculations of the enthalpy profile of this reaction. Clearly, larger basis sets are required to achieve a desirable level of accuracy. The nature of the potential energy surface particularly in the vicinity of the transition state can help to estimate the error of our calculations as well as to select methods using even a modest basis set in order to determine how to compute a more accurate potential energy surface.

The relative energy can be calculated according to the following equation using any (x) level of theory (e.g. x =

BH&HLYP) for the generation of a potential energy surface (4)

$$\Delta E_x = E_x(r_{\text{C}\cdots\text{HO}}, r_{\text{CH}\cdots\text{O}}) - [E_x(\text{propene}) + E_x(\text{OH})] \quad (4)$$

where $E_x(r_{\text{C}\cdots\text{HO}}, r_{\text{CH}\cdots\text{O}})$ represents the electronic energy of a given structure (determined by a pair of fixed variables: $r_{\text{C}\cdots\text{HO}}$ and $r_{\text{CH}\cdots\text{O}}$). The quantity of $[E_x(\text{propene}) + E_x(\text{OH})]$ stands for the total electronic energy of the structures of propene and OH radical, each being optimized at the x level of theory.

Figure 4 shows contour map presentations of potential energy surfaces (PESs), which illustrate the change of energy in the vicinity of the transition state of the reaction computed at various levels of theory. The minimum energy pathway (MEP) at the CCSD/6-31G(d) level of theory is denoted by the dotted line. Each diagram has contour lines as calibration for relative energy. Selected values of relative energies are shown to demonstrate the characteristics of a given PES. The progress of the reaction is made evident by clearly marking the reactant and product side of the PES at the top of the left-hand side and at the bottom of the right-hand side, respectively, in each of the figures.

Figure 4h illustrates the PES computed at the CCSD(T)/6-31G(d)//CCSD/6-31G(d) level of theory. This is the highest level of theory applied for the scan and is therefore assumed to be the closest to the “exact” surface. For this reason, it was used in all subsequent discussions as the reference surface. This figure shows that the electronic energy of the well-defined transition state is located between 35.0 and 37.5 kJ/mol.

It is clear from Figure 4 that there are some significant differences between the lower level PESs and the reference PES. In comparing the PESs generated at various levels of theory in each diagram of Figure 4, the large dot (●) and the dotted line symbolize the position of TS and MEP, respectively, on the reference PES {namely, CCSD(T)/6-31G(d)//CCSD/6-31G(d)}. The location of the TS (symbolized by ⊗) in HF-PES (denoted by a in Figure 4) is at 1.270 Å and 1.276 Å, $r_{\text{CH}\cdots\text{O}}$ and $r_{\text{C}\cdots\text{HO}}$, respectively. These values are also summarized in Table 2. We should note that the shape of the B3LYP surface (b) is significantly different from the remainder of PESs. Surprisingly, there is no transition state (TS) on this surface, as only a path or a channel was found instead of a well-localized TS. The TS (symbolized by ⊗) which belongs to the higher level MP2 ab initio calculation (denoted by c) occurs at 1.293 Å and 1.216 Å for $r_{\text{CH}\cdots\text{O}}$ and $r_{\text{C}\cdots\text{HO}}$, respectively. This suggests that at this level of theory, the correlation energy treatment shifts the position of the TS structure. The BH&HLYP surface (denoted by d) is an additional step toward the CCSD surface. Both $r_{\text{CH}\cdots\text{O}}$ (1.309 Å) and $r_{\text{C}\cdots\text{HO}}$ (1.224 Å) are larger than those associated with the MP2 surface. QCISD (denoted by e) and CCSD (denoted by f) are noticeably similar to each other. The shapes of these surfaces seem analogous: 1.327 Å and 1.231 Å for $r_{\text{CH}\cdots\text{O}}$ and $r_{\text{C}\cdots\text{HO}}$, respectively, in both cases. The QCISD(T) and CCSD(T) surfaces (denoted as g and h, respectively, in Figure 4) were generated on CCSD/6-31G(d) geometries with single point calculations and had no deviation in the geometric aspect.

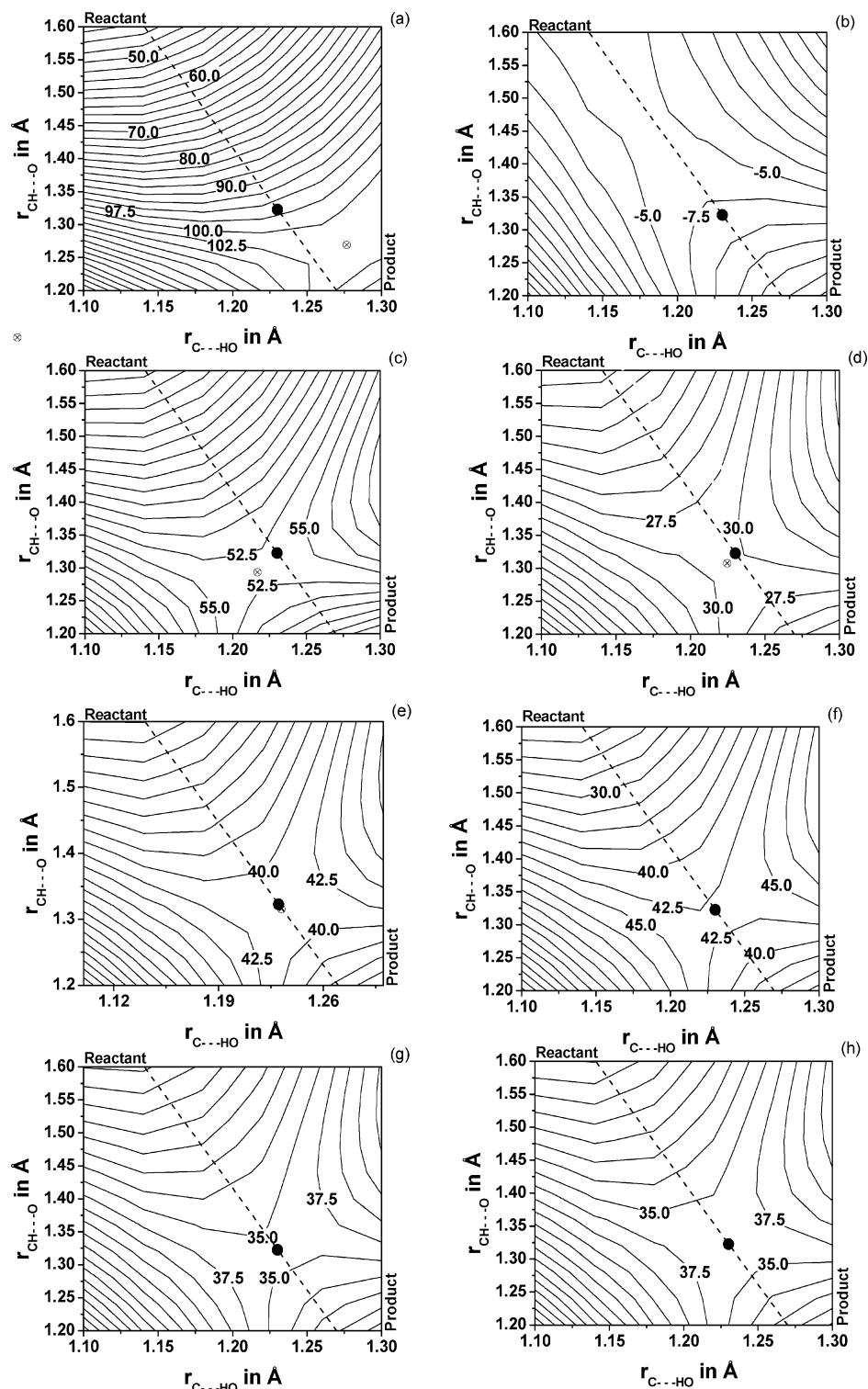


Figure 4. Potential energy surfaces (PES) around the TS of $\text{CH}_2=\text{CHCH}_3 + \bullet\text{OH} \rightarrow \text{CH}_2=\text{CHCH}_2\bullet + \text{H}_2\text{O}$ reaction computed at different levels of theory: (a) HF, (b) B3LYP, (c) MP2, (d) BH&HLYP, (e) QCISD, (f) CCSD, (g) QCISD(T), and (h) CCSD(T). The symbol \otimes indicates the place of the TS structure in the given method. The dotted line symbolizes the minimum energy pathway (MEP) and \bullet symbolizes the position of the TS obtained at the CCSD/6-31G(d) level of theory which is the “reference PES” (shown also in Figure 1).

The relative energies show remarkable deviations from the reference surface. The highest energy (101.5 kJ/mol) belongs to the TS structure found using the HF/6-31G(d) level of theory, as shown in the first diagram (a) in Figure 4. However, the relative energy difference was decreased by increasing the electron correlation: MP2, QCISD, and CCSD

(methods are denoted by c, e, and f of Figure 4, respectively) and the barrier heights were 52.8, 41.1, and 42.5 kJ/mol, respectively. Clearly, the deviation between the latter pair of values is not significant. The BH&HLYP surface (denoted by d of Figure 4) predicts the lowest barrier height of 29.6 kJ/mol among the calculated surfaces. It is interesting to note

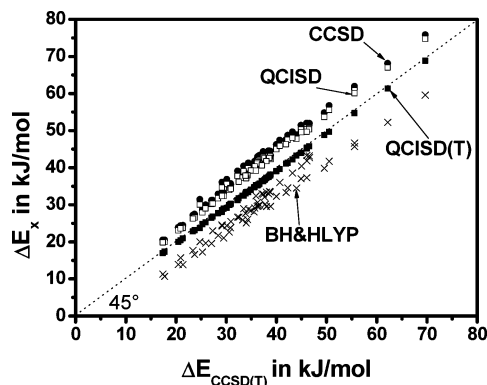


Figure 5. A comparison of relative energies obtained at the QCISD(T)/6-31G(d) (■), CCSD/6-31G(d) (●), QCISD/6-31G(d) (□), and BH&HLYP/6-31G(d) (×) levels of theory with respect to CCSD(T)/6-31G(d)//CCSD/6-31G(d) energies.

Table 3. Linear ($y = mx + b$) Fitted Parameters for the Correction of Relative Energy Values, Obtained at Various Levels of Theory against Relative Energies Computed at the CCSD(T)/6-31G(d) Level of Theory

model	m	b	R^2
HF	1.714	23.2	0.816
B3LYP	0.617	-102.8	0.741
MP2	1.178	5.7	0.942
BH&HLYP	0.946	-4.6	0.984
QCISD	1.052	2.3	0.997
CCSD	1.062	3.1	0.996
QCISD(T)	0.991	-0.5	0.999

that although the TS was not found on the B3LYP surface (b of Figure 4), it gave relative energy differences in the -5 and -7.5 kJ/mol range virtually at every grid point which are the closest to the experimental TS energy of -3.7 kJ mol⁻¹ (see Table 2).

The correlation of the different level of theories with relative CCSD(T)/6-31G(d) energies were examined. As Figure 5 shows, there is a noticeable correlation between the CCSD(T)/6-31G(d) and CCSD/6-31G(d) relative energies. Not surprisingly, the situation is the same with QCISD(T)/6-31G(d) and QCISD/6-31G(d). The fitting of BH&HLYP/6-31G(d) energy values to the CCSD(T)/6-31G(d) is also a good one. Linear fitting was carried out, as shown in (5)

$$\Delta E_x(r_{C\cdots HO}, r_{CH\cdots O}) = m\Delta E_{CCSD(T)}(r_{C\cdots HO}, r_{CH\cdots O}) + b \quad (5)$$

where x is QCISD(T), QCISD, CCSD, MP2, HF, BH&HLYP, and B3LYP. ΔE_x represents the relative energy calculated by the given method (x). The parameters m and b are fitted according to eq 5 and are summarized in Table 3. The correlation coefficient is up to 0.98 in the QCISD(T), QCISD, CCSD, and BH&HLYP cases indicating a relatively close approximation to the primary standard PES computed at the CCSD(T). At QCISD(T) the slope is the closest to unity: it is 0.991. In addition, the y-intercept is almost zero (-0.5 kJ/mol). However, QCISD and CCSD gave similar results for slope, but the deflection of the intercept increases to 2.3 and 3.1 kJ/mol, respectively. At BH&HLYP, the fitted parameter m is 0.946 which is slightly smaller, and parameter

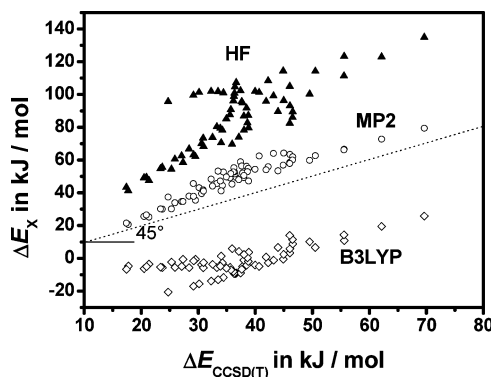


Figure 6. A comparison of relative energies obtained at the HF/6-31G(d) (▲), MP2/6-31G(d) (○), and B3LYP/6-31G(d) (◇) levels of theory with respect to CCSD(T)/6-31G(d)//CCSD/6-31G(d) energies.

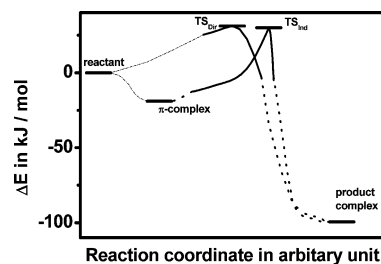


Figure 7. Relative BH&HLYP energy profile of indirect and direct H-abstractions: IRC calculation (solid curvature), normal optimization step (dotted curvature), and supplementary curvature (dash-dotted, thin line). Optimized critical points are represented by solid horizontal lines.

b is also somewhat lower at -4.6 kJ/mol. However, the remainder of the methods when plotted against CCSD(T) (Figure 6) do not show any obvious correlation, especially in the region between 20 and 50 kJ/mol of relative energies which corresponds to the value around the TS. In regards to these data the MP2 points show the best tendency for correlation in Figure 6, but the actual correlation coefficient of this linear fit is under 0.95.

4.1.3. Location of Reactant (π) and Product Complexes.

The fact that the experimental enthalpy of activation is negative (-3.7 kJ/mol) with respect to the reactant state (Table 2) means that H-abstraction should be relevant. The negative value of this activation enthalpy might predict that this reaction channel goes through a reactant or a π -complex of the OH plus propene and not via direct linear collision. However, one needs to address the question if it is possible to go from the π -complex to the TS of H-abstraction reaction as well as back to the separate reactants. Both direct and indirect H-abstraction channels were explored using IRC calculation at the BH&HLYP/6-31G(d) level of theory. Due to the numerical problem, these calculations were crashed after certain steps. The latest steps were used to optimize further (with the same level of theory) to reach the complexes. The indirect reaction pathway was followed along a long range using IRC (Figure 7). The latest point has energy under the reactant energy level by 12.6 kJ/mol. Consequently, there should be a prereaction complex for this channel. Then normal optimization was used to find it, and the π -complex

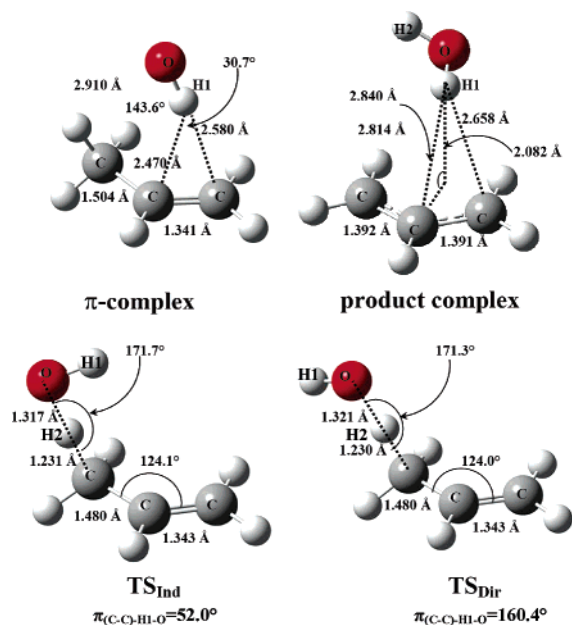


Figure 8. Top: Geometric parameters of reactant (so-called π), product complexes. Bottom: transition states (TS) for indirect and direct H-abstractions showing geometrical distinctions. All structure were computed at the CCSD/6-31G(d) levels of theory.

was characterized (Figure 8). The direct pathway was broken when OH was about 1.46 Å away from the hydrogen of the methyl group. Relative energy of this structure was 25.3 kJ/mol. The structures of these complexes were also determined by full geometry optimization at the CCSD/6-31G(d) level of theory. For both mechanisms, the same product complex was found (Figure 8).

In the π -complex, the hydroxyl radical with the hydrogen end is situated at the double bond 2.470 Å away from the central carbon. It means that the hydrogen is 0.11 Å closer than the terminal carbon of the ethylene group. The oxygen is orientated toward the hydrogen of the methyl group with a distance of 2.910 Å and an (O-H...C=) angle of 143.6° as indicated in Figure 8. This arrangement shows the relation to the H-abstraction. The single carbon-carbon bond has not changed at all when the π -complex is formed from the reactants (1.504 Å). The double bond has changed slightly (from 1.338 Å to 1.341 Å). A similar complex structure was obtained using the MP2/6-311G(d,p) level of theory by Vivier-Bunge et al.²⁰ This result can also confirm our BH&HLYP geometry. The product complex is very weakly bound and does not have a symmetric structure, which is depicted on the right-hand side of Figure 8. The water molecule is not in the symmetry plane of the allyl radical; however, carbon-carbon bond lengths are almost the same (1.392 Å and 1.391 Å). As is indicated in Figure 8, one of two hydrogens (H1) of the water molecule is at a 2.082 Å distance from the plane of the allyl radical. The other hydrogen (H2) and oxygen in the water molecule are closer to one end of the allyl radical than to the other. The distance between the central carbon atom and the hydrogen (H1) projected to the plane of allyl radical is 1.931 Å.

4.1.4. Details of Reaction Profiles around the Transition States. The IRCMax calculations are carried out on the

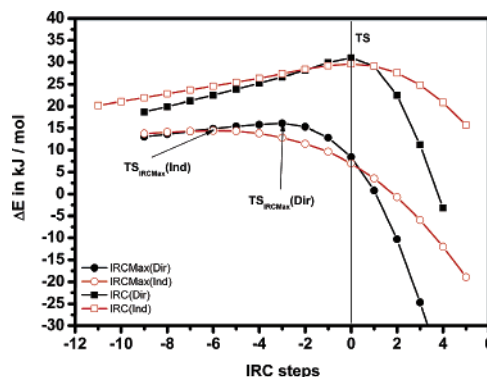


Figure 9. Comparisons of the IRC and IRCMax calculations at both direct (Dir) and indirect (Ind) channels. IRC and IRCMax were carried out at the BH&HLYP/6-31G(d) and QCISD(T)/6-311+G(3df,2p)//BH&HLYP/6-31G(d) levels of theory, respectively.

Table 4. Critical Geometric Parameters at the TS of Direct (TS_{Dir}) and Indirect (TS_{Ind}) Abstractions Computed at BH&HLYP/6-31G(d) and Obtained with the IRCMax Method

methods	$r_{C\cdots HO}$ (Å)	$r_{CH\cdots O}$ (Å)	E_{rel} (kJ/mol)
TS _{Dir}			
TS (BH&HLYP/6-31G(d))	1.224	1.314	31.1
TS (IRCMax)	1.119	1.443	16.1
TS _{Ind}			
TS (BH&HLYP/6-31G(d))	1.224	1.309	29.6
TS (IRCMax)	1.118	1.439	14.5

QCISD(T)/6-311+G(3df,2p)//BH&HLYP/6-31G(d) level of theory for both direct and indirect H-abstractions. The relative energies are related to the levels of propene and OH without zero-point correction, and they are calculated without counterpoise correction. The relative energies are plotted against the IRC steps as shown in Figure 9. The zeroth step is the transition state (TS) itself at the BH&HLYP/6-31G(d) level of theory in both cases of direct and indirect H-abstractions. In IRCMax calculations, the TS structures become considerably more reactantlike as Table 4 shows. If one compares the values of $r_{C\cdots HO}$ at the TS in IRCMax calculations (1.118 Å and 1.119 Å) with the experimental value of C-H bond in propene (1.117 Å), then these IRCMax calculations are not reasonable. The similarity of transition states at CCSD/6-31G(d) and at BH&HLYP/6-31G(d) also confirms that BH&HLYP geometry can be far more realistic. However, CCSD calculation at the larger basis set would give a more accurate structure of the TS, but these are very expensive to calculate. We also believe that the TS structures do not change so much.

4.1.5. Molecular Geometries. The deviation of BH&HLYP/6-31G(d) geometric parameters from the results obtained at the CCSD/6-31G(d) level of theory was studied in every grid point of the potential energy surface. For example, at the $r_{CH\cdots O} = 1.1$ Å and $r_{C\cdots HO} = 1.2$ Å point of the PES, the optimized parameter $r_{C=C}$ was 1.330 Å using the BH&HLYP method and 1.342 Å obtained by the CCSD level of theory, so the difference in $r_{C=C}$ was only 0.012 Å. Absolute

Table 5. Basis Set Effect on the Standard Activation and Reaction Enthalpies (in kJ/mol) for the $\text{CH}_2=\text{CHCH}_3 + \bullet\text{OH} \rightarrow \text{CH}_2\bullet\text{CHCH}_3 + \text{H}_2\text{O}$ Reaction Computed at the BH&HLYP/6-31G(d) Geometry

basis set	no. of basis functions	$\Delta_r H^\circ$	$\Delta^\ddagger H^\circ$
6-31G(d)	74	-87.9	18.8
cc-pVDZ	91	-101.4	8.8
6-311G(d,p)	114	-105.8	11.6
6-311+G(d)	130	-114.5	10.7
aug-cc-pVDZ	155	-118.8	6.7
6-311+G(3df,2p)	219	-118.4	10.2
cc-pVTZ	218	-113.1	10.6
aug-cc-pVTZ	345	-117.6	10.7
cc-pVQZ	430	-116.5	10.7

deviations were calculated using this process at each grid point of the BH&HLYP surface.

The above example illustrates that, in general, the agreement is good; the largest deviation (LD) was 0.015 Å in the bond lengths, 7.9° in the bond angles, and 6.3° in the dihedral angles. Note that these LD values belong to those extreme grid points of the PES which are at places far from the minimum energy pathway (MEP), and these points are actually very few in number. Consequently, BH&HLYP in combination with the 6-31G(d) basis set (Table 1) yields fairly accurate geometrical parameters with respect to those obtained by the CCSD/6-31G(d) computations.

4.2. Energetic Exploration of Reactants, Products, Complexes, and Transition States. 4.2.1. Basis Set Studies.

The effect of basis sets was also studied (see Tables 5 and 6). At the BH&HLYP/6-31G(d) geometry, single point calculations were carried out using various basis set sizes. As Table 5 shows, both reaction enthalpy ($\Delta_r H^\circ$) and activation enthalpy ($\Delta^\ddagger H^\circ$) tend to converge toward the experimental values, thus the results are qualitatively or semiquantitatively indicative. However, convergence is still limited for both $\Delta^\ddagger H^\circ$ (10.7 kJ/mol) and $\Delta_r H^\circ$ (-116.5 kJ/mol). The experimental result of reaction enthalpy is -128.53 kJ/mol⁶⁵⁻⁶⁷ which is 12.03 kJ/mol lower than the limit (-116.5 kJ/mol) of the BH&HLYP energy result. Unfortunately, there is relevant deviation between the BH&HLYP $\Delta^\ddagger H^\circ$ result (10.7 kJ/mol) and the experimentally estimated value (from -3.7 to +6.2 kJ/mol range depending on the extrapolation);⁷² the error is relatively large.

These results lead to higher level single point calculations such as QCISD(T) and CCSD(T) at medium 6-311G(d,p) and large 6-311+G(3df,2p) split valence basis sets on the CCSD/6-31G(d) geometries and BH&HLYP. Note that there is not only remarkable similarity between CCSD/6-31G(d) and BH&HLYP/6-31G(d) geometries, but energetic deviations at high level single point calculations are also negligible (about 1 kJ/mol). At these single point calculations of allyl radical and the transition state, the spin-momentum operator expectation values (S^2) are between 0.97 and 0.93. The QCISD(T) method can generally better handle the failure related to the spin contamination. Klippenstein et al.¹⁹ reported a similar value for the transition state of OH addition to ethene due to significant multireference character and/or dynamic correlation to the wave function. Their MRCI calculation compared to their QCISD(T) results shows agreement with each other. In the case of the hydroxyl radical, the expectation value of the S^2 operator is relatively close to 0.75, so the spin contamination may be considered acceptable in all cases. Table 5 presents the calculated reaction ($\Delta_r H^\circ$) and activation ($\Delta^\ddagger H^\circ$) enthalpies at different levels of theory.

BSSE was considered by the counterpoise method (see eq 3) both at the QCISD(T) and CCSD(T) levels of theory using 6-311G(d,p) and 6-311G+(3df,2p) basis sets: they are 23.2 and 10.3 kJ/mol for the activation enthalpy, for the two basis sets, respectively. In the case of the π -complex, BSSE was found to be moderate (6.4 and 3.9 kJ/mol) with those two basis sets. BSSE for the product complex were only 4.1 and 2.9 kJ/mol, respectively.

Both activation and reaction enthalpy change dramatically with the enhancement of the basis set (at the CCSD(T) and QCISD(T) level of theory). Using the 6-311G(d,p) basis set the stability of the π -complex decreases significantly. The activation enthalpy did not change for the direct abstraction, while extension of the basis set has a relevant effect on the indirect transition state: the barrier is decreased by 12 kJ/mol. Further increasing of the number of the basis set made the π -complex almost as stable as it was at 6-31G(d). The reaction enthalpy changes from the average of -108.5 kJ/mol to -124.7 kJ/mol. This effect probably is due to the formation of the allyl radical. This is a conjugated open shell system with a relevant multireference character. For comparison, the reaction G3MP2⁶⁸ enthalpy (-126.6 kJ/mol) and activation enthalpy for indirect abstraction (-1.6 kJ/mol)

Table 6. Basis Set Effect on the Stability of the π -Complex and the Product Complex as Well as Reaction and Activation Enthalpies Calculated (in kJ/mol) on CCSD/6-31G(d) Geometries

model	no. of basis functions	$\Delta H^\circ_{\pi\text{-complex}}$	$\Delta^\ddagger H^\circ$ direct	$\Delta^\ddagger H^\circ$ indirect	$\Delta H^\circ_{\text{product-complex}}$	$\Delta_r H^\circ$
CCSD(T)/6-31G(d)	74	-11.0	33.6	32.0	-96.3	-89.2
CCSD(T)/6-311G(d,p) ^a	114	-1.9	32.4	20.7	-106.1	-108.1
QCISD(T)/6-311G(d,p) ^a	114	-1.9	31.2	19.4	-107.0	-109.0
CCSD(T)/6-311+G(3df,2p) ^a	219	-7.1	7.3	1.9	-126.2	-123.8
QCISD(T)/6-311+G(3df,2p) ^a	219	-7.1	5.7	0.3	-127.2	-124.7
G3MP2/BHandHLYP ^b		-8.2	0.0	-1.6	-129.0	-126.6
exp. (from refs 63-66)				-3.7		-128.53

^a With the inclusion of BSSE correction (see eq 3) using the counterpoise method of Bernadi and Boys.⁵⁹ ^b G3MP2 enthalpy are calculated on the BH&HLYP/6-31G(d) geometry.

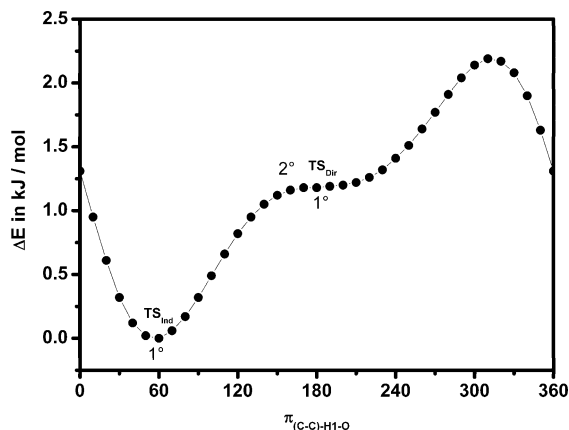


Figure 10. BH&HLYP/6-31G(d) potential energy curve along the $\pi_{C-C-H1-O}$ dihedral angle. The approximate position of the transition states and second-order saddle points are marked by 1° and 2° .

were calculated. They were found to be in good agreement with both the experimental and our high level data.

4.2.2. Search for Direct H-Abstraction TS and for a Second π -Complex. Since the first transition state optimized is associated with the path through the first π -complex, therefore it has to be classified as the TS for indirect H-abstraction (TS_{Ind}). Subsequently, the question of the existence of a second transition state corresponding to the direct H-abstraction (TS_{Dir}) must be examined. As our BH&HLYP/6-31G(d) geometry optimization shows, the relevant geometrical parameters for TS_{Dir} are similar to those of the indirect transition state (TS_{Ind}). Only the $r_{CH\cdots O}$ is by 0.004 \AA larger at TS_{Ind} , but it is only an insignificant difference. The H of the OH radical is orientated far away from the π -bond as the torsion angles ($\pi_{C-C-H1-O}$) were shown to be: 160.4° for the direct TS. That is 52.0° for the indirect TS. These two TS geometries are shown in the lower part of Figure 8; they appear to be rotamers. A semirigid rotational BH&HLYP/6-31G(d) potential along the $\pi_{C-C-H1-O}$ dihedral angle is shown in Figure 10. Clearly, at appropriately low temperature the TS_{Ind} will dominate the rate of the reaction. At sufficiently high temperature both transition states are involved. Note that the barrier that separates the TS_{Dir} and TS_{Ind} is in fact a second-order saddle point. However, the direct TS did not exhibit a linear structure, yet it did not have a prereaction complex in this channel as discussed before. In the possession of activation enthalpies and activation entropies one may estimate the relative rate constant of the indirect (IND) and direct (DIR) hydrogen abstraction:

$$\frac{k_{Ind}}{k_{Dir}} = \exp \frac{\Delta^\ddagger S_{Ind} - \Delta^\ddagger S_{Dir}}{R} \cdot \exp \frac{-(\Delta^\ddagger H_{Ind} - \Delta^\ddagger H_{Dir})}{RT} = \exp \frac{\Delta\Delta^\ddagger S}{R} \cdot \exp \frac{-(\Delta\Delta^\ddagger H)}{RT} \quad (6)$$

The calculation of the activation entropy can be made in two ways: (a) via the harmonic oscillator approximation for all of the normal modes and (b) via the hindered rotor treatment of the low frequencies and harmonic oscillator approximation for the remaining modes.

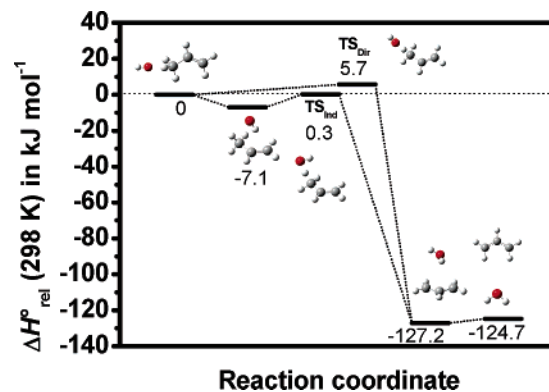


Figure 11. Enthalpy profile of the $CH_2=CHCH_3 + \bullet OH \leftrightarrow CH_2=CHCH_2\bullet + H_2O$ reaction. Enthalpies were obtained at the QCISD(T)/6-311+G(3df,2p)//CCSD/6-31G(d) level of theory. The sum of the enthalpies of formation of propene and the OH radical was chosen as the zero point for the enthalpy profile.

The difference in the activation entropy ($\Delta\Delta^\ddagger S$) is 6.1 J/(mol K) with harmonic oscillators approximation, while (b) method produces 10.9 J/(mol K) . They can increase the rate constant of the indirect H-abstraction related to the direct H-abstraction by a factor of 2.1 and 3.9, respectively. The activation enthalpy of the direct H-abstraction channel proved to be larger by 5.4 kJ/mol compared to those of the indirect TS calculated by the QCISD(T)/6-311+G(3df,2p)//CCSD/6-31G(d) level of theory. This difference makes the indirect abstraction 8.8 times faster than the direct one at room temperature. To summarize, the indirect H-abstraction reaction can be 18.3 (using harmonic oscillator approximation) and 32.2 (with hindered rotor treatment) times faster than the direct reaction at room temperature.

A systematic effort has been made to locate a second π -complex which could be associated with the OH addition. Since such a second π -complex has not been found, it seemed reasonable to assume that the one and only π -complex is a common intermediate for both the indirect H-abstraction and the OH addition.

4.2.3. Final Reaction Profile. Finally, we suggest, based on our extended study, that the activation enthalpy ($\Delta^\ddagger H^\circ$) of the title reaction should be 0.3 kJ/mol . The calculated reaction enthalpy ($\Delta_r H^\circ$) is -124.7 kJ/mol , which is in good agreement with the experimental value (-128.53 kJ/mol). Figure 11 shows the enthalpy profile of the reaction studied.

Alvarez-Idaboy et al. suggested^{20,21} an activation energy value of -8.78 kJ/mol , which is the result of their accurate PMP4/6-311+G(d,p)//MP2/6-311G(d,p) calculations,⁶⁹ as relative energy of addition channels compared to the entrance channel. This value is lower than the QCISD(T)/6-311G+(3df,2p) activation energy of the H-abstraction channel 3.1 kJ/mol which corresponds to the 0.3 kJ/mol activation enthalpy. Thus, addition reactions are probably faster than the H-abstraction in this case. However, both adducts have a fast unimolecular back reaction to the π -complex, and no subsequent reaction of the adducts exist²⁰ under the energy level of the propene+OH system. This is in contrast with the products of the H-abstraction.

5. Conclusions

The H-abstraction from propene with a hydroxyl radical was studied with different first principle computations, including B3LYP and BH&HLYP density functional methods (DFT), and HF, MP2, QCISD, QCISD(T), CCSD, and CCSD(T) ab initio methods combined with the 6-31G(d) split valence basis set, to explore the potential energy surface (PES) of the hydrogen abstraction reaction with special attention to the transition state and other stationary points. Relatively small deviations from the CCSD(T)/6-31G(d)//CCSD/6-31G(d) reference surface were found in the cases of the BH&HLYP, QCISD, QCISD(T), and CCSD level of theory. Linear relationships between the relative energies of these four and the reference methods have been found. The BH&HLYP method closely reproduces the geometrical parameters of the grid points of CCSD-PES, especially at the maxima and minima. It seems that the BH&HLYP method is very useful as it is a rapid way to compute reliable geometries for allylic H-abstraction. The BH&HLYP geometries of stationary points are not only similar to CCSD geometries but are also very close to available experimental data.

The energetic test shows that the BH&HLYP method tends to converge for both reaction and activation enthalpy as the basis set increases in size: $\Delta_r H^\circ = -117.0$ kJ/mol and $\Delta^\ddagger H^\circ = 10.7$ kJ/mol, respectively. There are acceptable deviations between the reaction and activation enthalpies obtained at the level of theory as was found previously.^{70,71}

We suggest a new value, based on our detailed ab initio analysis (QCISD(T)/6-311+G(3df,2p)//CCSD/6-31G(d), for the activation enthalpy of H-abstraction $\Delta^\ddagger H^\circ = 0.3 \pm 2.0$ kJ/mol (-3.7 and $+6.2$ kJ/mol experimental range⁷²). The calculated and the experimental reaction enthalpies are in good agreement: $\Delta_r H^\circ = -124.7 \pm 4.0$ kJ/mol and -128.53 kJ/mol, respectively.

Both the theoretical value of $\Delta^\ddagger H^\circ$ and the IRC calculation suggested that hydrogen abstraction is quite fast and predicted that the reaction cannot occur exclusively via direct collision but may eventuate also via a π -reactant complex intermediary. Although, the structures of the two H-abstraction transition states are quite similar, nevertheless their mechanisms show relevant differences. In addition, there is a competition between indirect H-abstraction as well as central and terminal additions. The structures of reactant (π) and product complexes were optimized, and their stabilities were computed.

Acknowledgment. The authors thank M. Labadi for technical support. One of the authors (I.G.C.) thanks the Ministry of Education for a Szent-Györgyi Visiting Professorship. The authors are grateful to the Hungarian Scientific Research Fund (OTKA T046861 and F037648). We wish to thank the University of Szeged (MU-00094/2002) for computational time.

Supporting Information Available: Important geometry parameters of H-abstraction obtained using different DFT and high level ab initio methods (Table S1). This

material is available free of charge via the Internet at <http://pubs.acs.org>.

References

- (1) Taatjes, C. A.; Hansen, N.; McIlroy, A.; Miller, J. A.; Senosiain, J. P.; Klippenstein, S. J.; Qi, F.; Sheng, L.; Zhang, Y.; Cool, T. A.; Wang, J.; Westmoreland, P. R.; Law, M. E.; Kasper, T.; Kohse-Höinghaus, K. *Science* **2005**, *308*, 1887–1889.
- (2) Braña, P.; Sordo, J. A. *J. Comput. Chem.* **2003**, *24*, 2044–2062.
- (3) Atkinson, R. *Chem. Rev.* **1986**, *86*, 69–201.
- (4) Atkinson, R. *J. Phys. Chem. Ref. Data* Monograph No. 1 1989.
- (5) Baulch, D. L.; Cobos, C. J.; Cox, R. A.; Frank, P.; Hayman, G.; Just, T.; Kerr, J. A.; Murrells, T.; Pilling, M. J.; Troe, J.; Walker, R. W.; Warnatz, J. *J. Phys. Chem. Ref. Data* **1994**, *23*, 847–1033.
- (6) Turpin, E.; Fittschen, C.; Tomas, A.; Devolder, P. *J. Atmos. Chem.* **2003**, *46*, 1–13.
- (7) Minetti, R.; Ribaucour, M.; Carlier, M.; Fittschen, C.; Sochet, L. R. *Combust. Flame* **1994**, *96*, 201–211.
- (8) Nagaoka, S.; Okauchi, Y.; Urano, S.; Nagashima, U.; Mukait, K. *J. Am. Chem. Soc.* **1990**, *112*, 8921–8924.
- (9) Chuong, B.; Stevens, P. S. *J. Phys. Chem. A* **2000**, *104*, 5230–5237.
- (10) Hippler, H.; Viskolcz, B. *Phys. Chem. Chem. Phys.* **2000**, *2*, 3591–3596.
- (11) Szilagy, I.; Dobe, S.; Berces, T.; Marta, F.; Viskolcz, B. *Z. Phys. Chem.* **2004**, *218*, 479–492.
- (12) Vakhit, A. B.; Lee, S.; Heard, D. E.; Smith, I. W. M.; Leone, S. R. *J. Phys. Chem. A* **2001**, *105*, 7889–7895; **2003**, *107*, 10055–10062.
- (13) Walch, S. P. *J. Chem. Phys.* **1993**, *98*, 3163–3178.
- (14) Zellner, R.; Lorenz, K. *J. Phys. Chem.* **1984**, *88*, 984–989.
- (15) Spangenberg, T.; Köhler, S.; Hansmann, B.; Wachsmuth, U.; Abel, B. *J. Phys. Chem. A* **2004**, *108*, 7527–7534.
- (16) Vereecken, L.; Peeters, J. *Chem. Phys. Lett.* **2001**, *333*, 162–168.
- (17) Bradley, J. N.; Hack, W.; Hoyer, K.; Wagner, H. G. *J. Chem. Soc., Faraday Trans. 1* **1973**, *69*, 1889–1898.
- (18) Diau, E. W. G.; Lee, Y. P. *J. Chem. Phys.* **1992**, *96*, 377–386.
- (19) Greenwald, E. E.; North, S. W.; Georgievskii, Y.; Klippenstein, S. J. *J. Phys. Chem. A* **2005**, *109*, 6031–6044.
- (20) Diaz-Acosta, I.; Alvarez-Idaboy, J. R.; Vivier-Bunge, A. *Int. J. Chem. Kinet.* **1999**, *31*, 29–36.
- (21) Alvarez-Idaboy, J. R.; Diaz-Acosta, I.; Vivier-Bunge, A. *J. Comput. Chem.* **1998**, *19*, 811–819.
- (22) Atkinson, R.; Arey, J. *Chem. Rev.* **2003**, *103*, 4605–4638.
- (23) Chen, W.; Schlegel, H. B. *J. Chem. Phys.* **1994**, *101*, 5957–5968.
- (24) Henry, D. J.; Parkinson, C. J.; Radom, L. *J. Phys. Chem. A* **2002**, *106*, 7927–7936.
- (25) Kohn, W.; Becke, A. D.; Parr, R. G. *J. Phys. Chem.* **1996**, *100*, 12974–12980.

- (26) Ziegler, T. *Chem. Rev.* **1991**, *91*, 651–667.
- (27) Handy, N. C.; Tozer, D. J.; Lamming, G. J.; Murray, C. W.; Amos, R. D. *Isr. J. Chem.* **1993**, *33*, 331–344.
- (28) Johnson, B. G.; Gill, P. M.; Pople, J. A. *J. Chem. Phys.* **1993**, *98*, 5612–5626.
- (29) Baker, J.; Scheiner, A.; Andzelm, J. *Chem. Phys. Lett.* **1993**, *216*, 380–388.
- (30) Lamming, G. J.; Handy, N. C.; Amos, R. D. *Mol. Phys.* **1993**, *80*, 1121–1134.
- (31) Curtiss, L. A.; Raghavachari, K.; Redfern, P. C.; Pople, J. A. *J. Chem. Phys.* **1997**, *106*, 1063–1079.
- (32) Fan, L. Y.; Ziegler, T. *J. Am. Chem. Soc.* **1992**, *114*, 10890–10897.
- (33) Durant, J. L. *Chem. Phys. Lett.* **1996**, *256*, 595–602.
- (34) Lynch, B. J.; Truhlar, D. G. *J. Phys. Chem. A* **2001**, *105*, 2936–2941.
- (35) Bacskay, G. B. *Chem. Phys.* **1981**, *61*, 385–404.
- (36) Hariharanm, P. C.; Pople, J. A. *Theor. Chim. Acta* **1973**, *28*, 213–222.
- (37) Roothan, C. C. J. *Rev. Mod. Phys.* **1951**, *23*, 69.
- (38) Pople, J. A.; Nesbet, R. K. *J. Chem. Phys.* **1954**, *22*, 571–572.
- (39) McWeeny, R.; Dierksen, G. *J. Chem. Phys.* **1968**, *49*, 4852–4856.
- (40) Moller, C.; Plesset, M. S. *Phys. Rev.* **1934**, *46*, 618.
- (41) Head-Gordon, M.; Pople, J. A.; Frisch, M. J. *Chem. Phys. Lett.* **1988**, *153*, 503–506.
- (42) Frisch, M. J.; Head-Gordon, M.; Pople, J. A. *Chem. Phys. Lett.* **1990**, *166*, 275–280.
- (43) Saebo, S.; Almlof, J. *Chem. Phys. Lett.* **1989**, *154*, 83–89.
- (44) Pople, J. A.; Head-Gordon, M.; Raghavachari, K. *J. Chem. Phys.* **1987**, *87*, 5968–5975.
- (45) Cizek, J. *Adv. Chem. Phys.* **1969**, *14*, 35.
- (46) Purvis, G. D.; Bartlett, R. J. *J. Chem. Phys.* **1982**, *76*, 1910–1918.
- (47) Scuseria, G. E.; Janssen, C. L.; Schaefer, H. F., III *J. Chem. Phys.* **1988**, *89*, 7382–7387.
- (48) Scuseria, G. E.; Schaefer, H. F., III *J. Chem. Phys.* **1989**, *90*, 3700–3703.
- (49) Hohenberg, P.; Kohn, W. *Phys. Rev.* **1964**, *136*, B864.
- (50) Stephens, P. J.; Devlin, F. J.; Chabalowski, C. F.; Frisch, M. J. *J. Phys. Chem.* **1994**, *98*, 11623–11627.
- (51) Becke, A. D. *J. Chem. Phys.* **1993**, *98*, 5648–5652.
- (52) Note that BH&HLYP means $0.5 \times E_X^{\text{HF}} + 0.5 \times E_X^{\text{LSDA}} + 0.5 \times \Delta E_X^{\text{Becke88}} + E_C^{\text{LYP}}$ functional.
- (53) Scaling factors for ZPVE: HF(0.9135), MP2(0.9670), QCISD-(0.9776), and B3LYP(0.9806) from the following: Scott, A. P.; Random, L. *J. Phys. Chem.* **1996**, *100*, 16502–16513.
- (54) Woon, D. E.; Dunning, T. H., Jr. *J. Chem. Phys.* **1993**, *98*, 1358–1371.
- (55) Kendall, R. A.; Dunning, T. H., Jr.; Harrison, R. J. *J. Chem. Phys.* **1992**, *96*, 6796–6806.
- (56) Dunning, T. H., Jr. *J. Chem. Phys.* **1989**, *90*, 1007–1023.
- (57) Peterson, K. A.; Woon, D. E.; Dunning, T. H., Jr. *J. Chem. Phys.* **1994**, *100*, 7410–7415.
- (58) Wilson, A.; van Mourik, T.; Dunning, T. H., Jr. *J. Mol. Struct. (THEOCHEM)* **1996**, *388*, 339–349.
- (59) Boys, S. F.; Bernardi, F. *Mol. Phys.* **2002**, *100*, 65–73.
- (60) Malick, D. K.; Petersson, G. A.; Montgomery, J. A., Jr. *J. Chem. Phys.* **1998**, *108*, 5704.
- (61) Frisch, M. J.; Trucks, G. W.; Schlegel, H. B.; Scuseria, G. E.; Robb, M. A.; Cheeseman, J. R.; Montgomery, J. A., Jr.; Vreven, T.; Kudin, K. N.; Burant, J. C.; Millam, J. M.; Iyengar, S. S.; Tomasi, J.; Barone, V.; Mennucci, B.; Cossi, M.; Scalmani, G.; Rega, N.; Petersson, G. A.; Nakatsuji, H.; Hada, M.; Ehara, M.; Toyota, K.; Fukuda, R.; Hasegawa, J.; Ishida, M.; Nakajima, T.; Honda, Y.; Kitao, O.; Nakai, H.; Klene, M.; Li, X.; Knox, J. E.; Hratchian, H. P.; Cross, J. B.; Bakken, V.; Adamo, C.; Jaramillo, J.; Gomperts, R.; Stratmann, R. E.; Yazyev, O.; Austin, A. J.; Cammi, R.; Pomelli, C.; Ochterski, J. W.; Ayala, P. Y.; Morokuma, K.; Voth, G. A.; Salvador, P.; Dannenberg, J. J.; Zakrzewski, V. G.; Dapprich, S.; Daniels, A. D.; Strain, M. C.; Farkas, O.; Malick, D. K.; Rabuck, A. D.; Raghavachari, K.; Foresman, J. B.; Ortiz, J. V.; Cui, Q.; Baboul, A. G.; Clifford, S.; Cioslowski, J.; Stefanov, B. B.; Liu, G.; Liashenko, A.; Piskorz, P.; Komaromi, I.; Martin, R. L.; Fox, D. J.; Keith, T.; Al-Laham, M. A.; Peng, C. Y.; Nanayakkara, A.; Challacombe, M.; Gill, P. M. W.; Johnson, B.; Chen, W.; Wong, M. W.; Gonzalez, C.; Pople, J. A. *Gaussian 03, revision C.02*; Gaussian, Inc.: Wallingford, CT, 2004.
- (62) *CRC Handbook of Chemistry and Physics*, 77th ed.; Lide, D. R., Frederikse, H. P. R., Eds.; CRC Press: Boca Raton, FL, 1996–1997.
- (63) *JANAF Thermochemical Tables*, 3rd ed.; Chase, M. W., Jr., Davies, C. A., Downey, J. R., Frurip, D. J., McDonald, R. A., Syverud, A. N., Eds.; National Bureau of Standards: Washington, DC, 1985; Vol. 14.
- (64) Hirota, E.; Yamada, C.; Okunishi, M. *J. Chem. Phys.* **1992**, *7*, 2963–2970.
- (65) Turányi, T.; Zalotai, L.; Dóbbé, S.; Bérces, T. *Phys. Chem. Chem. Phys.* **2002**, *4*, 2568–2578.
- (66) Ruscic, B.; Boggs, J. E.; Burcat, A.; Császár, A. G.; Demaison, J.; Janoschek, R.; Martin, J. M. L.; Morton, M. L.; Rossi, M. J.; Stanton, J. F.; Szalay, P. G.; Westmoreland, P. R.; Zabel, F.; Bérces, T. *J. Phys. Chem. Ref. Data* **2005**, *34*, 573–656.
- (67) Frenkel, M.; Marsh, K. N.; Wilhoit, R. C.; Kabo, G. J.; Roganov, G. N. *Thermodynamics of Organic Compounds in the Gas State*; Thermodynamics Research Center: College Station, TX, 1994.
- (68) Baboul, A. G.; Curtiss, L. A.; Redfern, P. C.; Raghavachari, K. *J. Chem. Phys.* **1999**, *110*, 7650.
- (69) Krishnan, R.; Pople, J. A. *Int. J. Quantum Chem.* **1978**, *14*, 91–100.
- (70) Truong, T. N.; Duncan, W. *J. Chem. Phys.* **1994**, *101*, 7408–7414.
- (71) Durant, J. L. *Chem. Phys. Lett.* **1996**, *256*, 595–602.
- (72) Tsang, W. *J. Chem. Ref. Data* **1991** 221–273. They proposed for rate constant for the reaction studied as follows: $k(T) = 2.8 \times 10^{11} (T/298)^2 \cdot \exp(1.25 \text{ kJ}/RT) \text{ cm}^3/(\text{molecule} \cdot \text{s})$, where $T = 300\text{--}2500 \text{ K}$ and uncertainty = 1.20.